Intermetallics 158 (2023) 107884

Contents lists available at ScienceDirect

Intermetallics

journal homepage: www.elsevier.com/locate/intermet

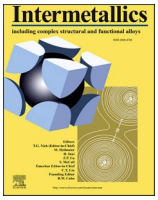

Integrating HIP and homogenisation heat treatment and its effect on the workability of a conventional peritectic TiAl alloy

Sean Peters *, Marcos Perez, Paul Blackwell

Advanced Forming Research Centre, University of Strathclyde, 85 Inchinnan Drive, Inchinnan, Renfrew, PA4 9LJ, UK

ARTICLE INFO

Keywords:
Intermetallics
Dynamic recrystallisation
Anisotropy
Isothermal forging
Hot isostatic pressing
Microstructure

ABSTRACT

The aim of this study was to understand how consolidation and homogenisation, as well as the possibility of integrating the two processes, influences the pre-compression microstructure and subsequent compression behaviour of an industry accepted, peritectic solidifying titanium aluminide ingot alloy; 45XD.

This study differs from existing work with its emphasis on understanding the effect of integrating consolidation and homogenisation on workability, as well as how these processes influence the pre-and post-compression microstructure individually. This was assessed by the material's strain rate sensitivity in primary and secondary compression. The target microstructure was identified from the literature as being capable of a strain rate sensitivity of $\geq$0.3.

The results presented here show that it is possible to integrate the consolidation and homogenisation stages, and this proved beneficial, namely achieving a high lamellar content and elementally homogeneous microstructure presented prior to compression. Subsequent deformation generated high values of dynamic recrystallisation fraction and globularisation returned upon primary compression, and the highest strain rate sensitivity at secondary compression, in comparison to material processed by the traditional approach. This is thought to be due to pressure and temperature during the integrated process reducing both segregation, seen through casting, and so the B2/β_0 content compared to consolidated material. The integrated consolidation and homogenisation approach also prevented the grain growth seen in the traditional route; this is anticipated to be due to the two slow cooling stages involved in the traditional process rather than the effect of isostatic pressure.

1. Introduction

Titanium aluminide (TiAl) alloys fill an important gap between high temperature and high-density superalloys and low temperature and low-density titanium and aluminium alloys. This is particularly important when considering high temperature applications such as automotive and aerospace engine components [1]. Titanium aluminides compare favourably to nickel-based superalloys in terms of their high elastic modulus and low density, and to titanium alloys in terms of high temperature stability and oxidation resistance [2].

One major obstacle to further application is in the processing of a material with an inherent brittle nature at low temperatures (<800 °C). This leads to wrought processing techniques being largely avoided due to the high processing and equipment costs involved in multiple processing steps working at elevated temperatures which are necessary to achieve acceptable workability, as reviewed by Appel et al. [3]. The poor ductility during hot working is linked to issues inherent in the material i.e., from the lack of slip systems in the long range ordered phases present at room and working temperatures. There are also challenges created by the casting process namely large lamellar grain sizes and elemental segregation. Therefore, reducing processing steps whilst improving forging outcomes would be of industrial interest.

Hot isostatic pressing (**HIP**) is an essential step applied to remove solidification porosity. However, simple HIP and single stage primary uniaxial compression (i.e. forming a pre-form or ingot upsetting) has been shown to not remove the anisotropy-causing lamellar grains and casting segregation, which are known to hinder secondary processing stages, such as isothermal closed die forging and hot rolling [4–9].

To ensure successful and homogeneous compression *Semiatin* et al. found that heating is required at temperatures in the α phase before wrought processing [10,11]. They identified that if ingot material had not been held above the α transus, aluminium segregation from casting caused issues such as variable transus temperatures, flow stresses and phase distribution upon compression. This was also noted by *Fuchs* [12].

* Corresponding author.
E-mail addresses: sean.peters@strath.ac.uk (S. Peters), marcos.perez@strath.ac.uk (M. Perez), paul.blackwell@strath.ac.uk (P. Blackwell).

https://doi.org/10.1016/j.intermet.2023.107884
Received 12 December 2022; Received in revised form 28 February 2023; Accepted 14 March 2023

This work has been followed by other researchers espousing the importance of the >α transus homogenisation (**HMG**) step for processing; elemental homogeneity and refined fully lamellar microstructures increasing the extent of dynamic recrystallisation (**DRX**) fraction upon compression, referred to as globularisation in this study and calculated by the grain orientation spread approach [13–18]. The deformation mechanisms of these fully lamellar microstructures were discussed by Palomares-Garcie et al.[19].

As well as lamellar microstructures of γ and α_2 phases, 45XD (Ti–44Al–2Nb–3Mn–1B at%, exothermic dispersion of boride, XD). also contains the ordered B2/β_0 phase, without the benefit to workability of solidifying through the single, disordered β phase region [17,18]. The β phase fraction (B2/β_0) is accentuated by segregation [20]. At the lower working temperatures used in this study, also examined by Tetsui et al. and others, the long range ordered version of the β structure (B2/β_0) is present [21–23]. This has limited deformability due to the loss of symmetry seen in the unit cell upon ordering and β_0 concentrates dislocation pile-ups, as identified by Molénat et al., its presence contributing little to workability [24]. Workable β only comes with the disordering reaction of $\beta_o \rightarrow \beta$ at high temperatures, as was shown on TiAl alloy Ti-43.5Al–4Nb–1Mo-0.1B in TNM by Schwaighofer et al. [15]. The disordering reaction temperature for 45XD is not known.

As found by Zhang, Dehm and Clemens, removing the β_o phase isn't without its difficulties [25]. Investigations of the impact of HIP and HMG on the content and distribution of this phase found both pressure and α phase HMG essential to removing B2/β_o but this came with excessive grain growth in their low boride alloy.

Regarding the above, the traditional HIP and >α transus homogenisation (**THH**) stages are deemed necessary to improve microstructural outcomes from primary compression. However, HMG is often avoided due to the costs linked with vacuum heat treatment and/or excessive grain growth. Integrating HIP and HMG (subsequently referred to as **IHH**), using HIP equipment for both stages, has been investigated as an alternative approach [26]. Chen et al. concluded that the isostatic pressure had no bearing on morphology evolution, but suppressed microcrack formation, which proved beneficial in their study on mechanical performance.

To assess potential workability of HIP, THH and IHH processes for 45XD, strain rate sensitivity (***m***) indexing (0–1, 0 being least sensitive, 1 being most) is used to assess primary and, most importantly, secondary compression [27]. The *m* value incorporates both macroscopic and microscopic plastic deformation behaviour, (e.g. lamellar grain globularisation or orientation and dislocation concepts, respectively) for that particular microstructure, *m* values for TiAl in compression were assessed by Bibhanshu et al. [28]. Materials with low *m* microstructures during processing can suffer localised deformation. This inhomogeneous deformation behaviour can lead to failure, so processing conditions where *m* is high are preferred, this being supported by process mapping [29]. Gupta et al. identify 0.2–0.3 as satisfactory for typical forming operations, *Fuchs* suggested *m* of ≥0.3; both found increasing temperature usually resulted in an increase of *m* in their compression trials mapping the alloy Ti–48Al–2Cr–2Nb (4822) [4,30]. However, *Gupta* et al. begin by identifying that intrinsic workability still depends on the initial microstructure and its response to temperature, strain rate and strain. Forging trials on boride free Ti–45Al alloy by *Seetharaman and Semiatin,* found that *m* and the fraction of globularised lamellar material increased with a lower initial lamellar grain size, as did *Fuchs* with 4822 alloy, so this relationship between *m* in compression and microstructure is well established [31]. For this reason, temperature remains constant in the present work, as the effect of IHH on microstructure and subsequent *m* is investigated. This study will use *m* of ≥0.3 as a target.

To summarise, simple HIP has repeatedly been shown not to produce microstructures best placed for optimising the microstructural outcome of uniaxial compression, with globularisation resistant lamellar grains, and casting segregation hindering secondary processing [5]. The work reported here evaluates the effect of pre-compression consolidation and homogenisation on 45XD as well as the option of integrating the process, and its effect on workability.

2. Material and experimental methods

Cast plasma arc melted ingot 45XD alloy was cut via electrical discharge machining (**EDM**) into three cylindrical samples of Ø60 × 200 mm to provide material in three different starting conditions. The composition data used for calculating the phase diagram (CALPHAD, Fig. 1b), was determined via inductively coupled plasma (**ICP**), Table 1. The phase diagram was used to inform the processing conditions for this alloy. Two of these cylinders were consolidated via HIP for 4 h at 1270 °C, 175 MPa under argon. This is referred to as the HIP condition. One of these cylinders was further homogenised at 1300 °C for 2 h under vacuum, referred to as traditional HIP and homogenised material (**THH**). The remaining cylinder was consolidated using the same HIP conditions, but following the HIP cycle and before cooling, the temperature was ramped up to reach the homogenisation temperature of 1300 °C for 2 h, maintaining pressure in the vessel throughout. This material is referred to as the integrated HIP and homogenised (**IHH**).

All sample material was then cut into cylindrical compression samples of Ø13 × 20 mm, again via EDM for primary (1') compression, to replicate ingot breakdown, or forming a pre-form.

For the primary (**1'**) compression trials, the cylindrical samples were coated with glass-based lubricant and the compression platens lubricated with boron nitride before reduction to 50% at 1100 °C (γ+β phase region) after a 5-min soak, with different strain rates at 0.001, 0.005 and 0.01 s^{-1} to establish the strain rate sensitivity (***m***) of the material, this using a Zwick-Roell Z250kN screw-drive machine.

For secondary (**2″**) compression, only samples that were 1′ compressed at 0.001 s^{-1} were used to produce 2″ compression samples via EDM of Ø6x9 mm cylinders. The 2" compression conditions followed the same procedure as the 1' compression stage, at 1100 °C, but at strain rates of 0.001, 0.01 and 0.1 s^{-1} to establish the *m* value of the material.

Following metallurgical preparation, microstructural analysis included optical microscopy (**OM**) and scanning electron microscopy (**SEM**) in back-scattered electron (**BSE**) mode at 15–20 kV. OM and BSE images were analysed via ImageJ software to determine microstructural parameters including average lamellar grain area (μm^2), via a method applied by *Kościelna and Szkliniarz*, and lamellar content (%) via ASTM E562-19e1 [13]. Electron back-scatter diffraction (**EBSD**) was used to assess phase fraction and grain area fraction ≤50 μm^2 through mapping the microstructure, the dynamic recrystallised fraction (X-DRX) was calculated through the grain orientation spread (**GOS**) approach, all through MTEX. To define a grain, 10° of misorientation was used. A similar methodology for estimating microstructural constituents and phase fraction was applied using image processing tools on BSE micrographs by Schwaighofer et al. [15].

3. Results

3.1. Pre-compression microstructure

Microstructural analysis was conducted on 45XD in the three starting material conditions already discussed; HIP, THH and IHH, to assess the influence of initial microstructure on compression behaviour and the resulting microstructural evolution post 1' compression.

Fig. 2 BSE imaging compares the three pre-compression microstructures. Pre-compression, each of HIP, THH and IHH returns a nearly fully lamellar microstructure, with β phase present as grains at lamellae grain boundaries as well as within the lamellar laths, most prominently in the HIP material at 2.9 β_{eq}% and 6.3 β_{lam}% respectively. This is higher than both THH and IHH, as shown in Table 2, which quantifies these microstructural characteristics from BSE and EBSD image processing. Lamellar content for HIP and THH is similar at 68.9 and 74.8% respectively, IHH resulting in higher lamellar content of 90.3%. The

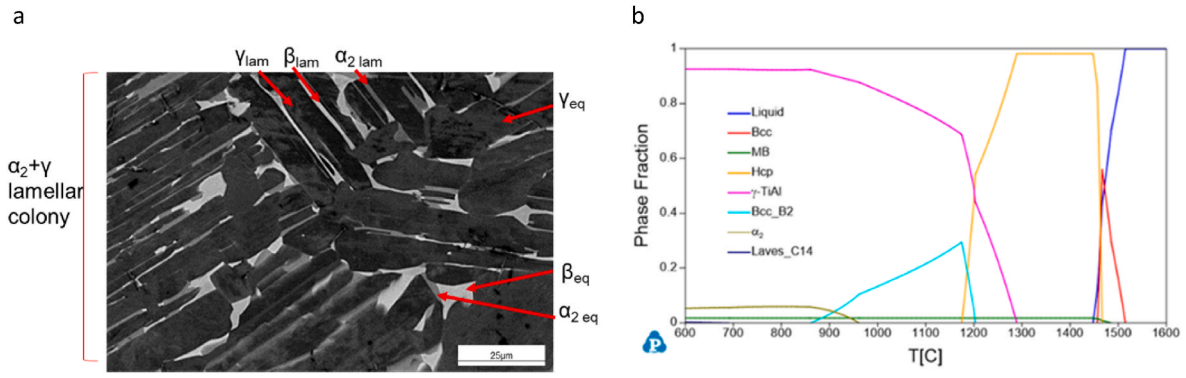

Fig. 1. (a) SEM image of HIP microstructure to identify phases and lamellar (lam) and equiaxed (eq) microstructures, as indicated dark grey/black areas correspond to γ phase, white β and light grey α_2, (b) phase fraction diagram determined from CALPHAD, with main crystal structures (including metallic boride (MB)).

Table 1
Average chemical composition of supplied 45XD ingot, analysed via ICP at three points.

Ti	Al	Nb	Mn	B	O	Fe	Cu	C	N	Si
49.80	44.31	1.93	2.93	0.84	0.10	0.02	0.03	0.02	0.01	0.02

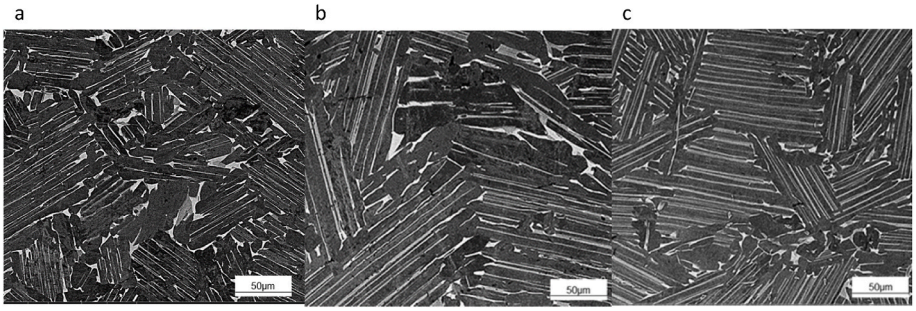

Fig. 2. BSE images of 45XD alloy in the HIP (a), THH (b), IHH (c) condition at 500x magnification. Dark grey areas correspond to γ phase, white β and light grey α_2.

Table 2
Phase morphology fraction and lamellar content in the three material conditions of 45XD before compression.

45XD material condition	α_2 lam (%)	β lam (%)	γ lam (%)	α_2 eq (%)	β eq (%)	γ eq (%)	Lamellar content (%)
HIP	4.4	6.3	51.7	2.0	2.9	23.3	68.9
THH	0.9	2.4	62.1	0.3	0.8	20.9	74.8
IHH	8.8	2.4	65.0	1.0	0.3	7.0	90.3

lamellar grain area details for each condition show large grains present, >1000 μm^2, the largest being for THH, which also shows a higher interquartile spread than for HIP and the IHH; Fig. 3. The smallest grain area with the tightest interquartile spread was in the IHH material. The associated γ_{lam}% rises with lamellar content in IHH, this being 65.0% versus 51.7% in HIP and γ_{eq}% decreases from 23.3% compared to 7.0%.

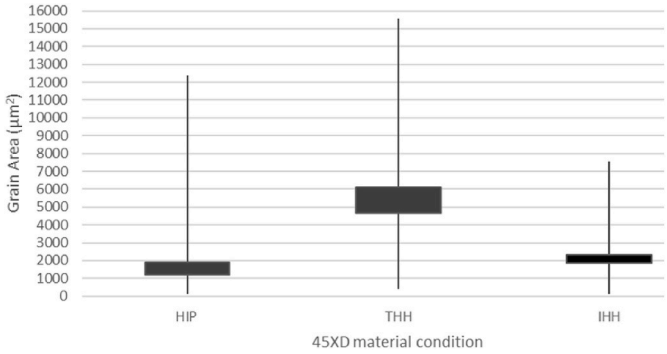

Fig. 3. Lamellar grain area analysis of maximum, minimum and interquartile range of each material starting condition.

3.2. Primary compression

3.2.1. Primary compression behaviour

Each stress-strain curve follows a similar pattern, with strain hardening followed by peak flow stress (σ_{pfs}), rising with increase in strain rate (ε), this being followed by flow softening; shown in Fig. 4a. Flow softening at all $\dot{\varepsilon}$ suggests that there was time for microstructural breakdown to occur as strain increased. From the slope of Fig. 4b, the unitless strain rate sensitivity (m) can be estimated with Eq (1); see detail in Table 3.

$$m = \frac{d(ln\ \sigma_{pfs})}{d(ln\dot{\varepsilon})} \quad (1)$$

IHH shows the highest m value at 0.29, HIP showing the lowest from σ_{pfs} in 1′ compression at 0.21. From the compression stress-strain curves for 1′ compression, once a strain (ε) of 0.7 is reached IHH consistently shows the lowest value of σ, for each strain rate and material. This being the case even with the highest flow stress at 0.01 s^{-1} with the largest degree of flow softening seen. All material conditions show stable

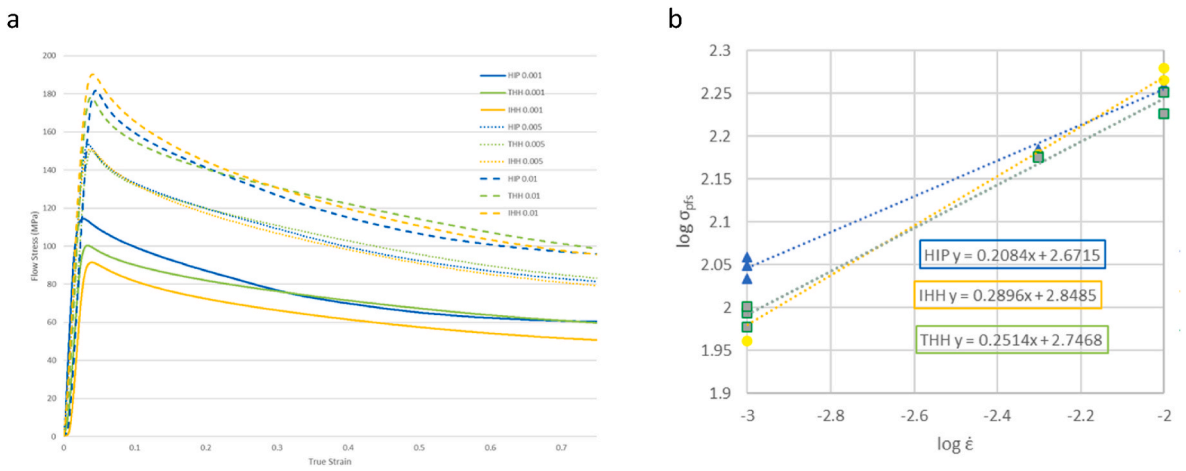

Fig. 4. Primary stress-stain curves (a), compression at 1100 °C to 50% at 0.001, 0.005 and 0.01 s^{-1} over 760, 152, and 76 s respectively. Calculation of strain rate sensitivity (m) for each material for primary compression (b).

Table 3
Peak flow stress and strain rate sensitivity, measured at peak flow stress, strain of 0.04, for each material condition over primary compression.

45XD Material condition	HIP			THH			IHH		
Strain rate (s^{-1})	0.001	0.005	0.01	0.001	0.005	0.01	0.001	0.005	0.01
1′ σ_{pfs}- (MPa)	111.5	153.3	181.7	97.9	149.9	173.3	95.9	150.3	187.4
1′ m (σ_{pfs})	0.21			0.25			0.29		

material flow under these 1' compression conditions.

3.2.2. *Primary compression microstructure*

As the mapping in Fig. 5 illustrates, all processing conditions returned successfully compressed material, though each starting state returned material still containing some lamellar morphologies after 1' compression.

The content and details of these morphologies are shown in.

Fig. 6. Phase fraction and morphology details in Table 4 for compressed material show a reduction in lamellar content and the respective morphologies from pre-compression for all material conditions. However, an increase in overall β content for IHH and THH conditions with compression was seen. The β_{eq} content increased from below 1%, to 4.0% and 7.0% for THH and IHH respectively. The HIP phase fraction stayed relatively constant with a small increase from 2.9% to 5.2% for 0.001s^{-1}. This could be related to compression temperature.

Concerning the material deformed with strain rate of 0.001 s^{-1}, the most effective strain rate for dynamic globularisation, IHH returned the highest X-DRX and "grains ≤50 μm^2" fraction at 67.1% and 68.3%, with the lowest overall lamellar content at 18.9%, these lamellar structures being of the smallest grain area.

THH material shows the highest lamellar content at 45.6%, with the largest spread of lamellar grain area as well as the lowest X-DRX and "grains ≤50 μm^2" fraction at 29.6% and 42% respectively, versus 52.8% and 57.1% for HIP.

For IHH at faster strain rates of 0.005 and 0.01 s^{-1}, the trend is for X-DRX to reduce, to 37.8% and 31.7%, respectively and the lamellar fraction to increase to 38.9% and 56.1%. For HIP and THH at these strain rates the trend is less clear, as shown by Table 4.

Lamellar grain details shown in.

Fig. 6, again show a trend with increasing strain rate returning larger lamellar grain sizes, with less homogeneity of size for IHH material. There is no clear trend for the HIP and THH conditions.

The X-DRX indicated in Table 4, was calculated for all strain rates via the GOS approach. This is shown in Fig. 7a, c, e for 0.001 s^{-1} processed material. Following this method, those grains with less than or equal to 2° spread within the grain are deemed to have been recrystallised, above this they are considered deformed. In addition to this, the grain area frequency, is shown in Fig. 7b, d, f, for HIP, THH and IHH respectively, this also includes the fraction of the "grains ≤50 μm^2"; another measure for further workability in the next processing stage.

3.3. *Secondary compression*

3.3.1. *Secondary compression behaviour*

The 2" compression stress-strain curves at Fig. 8a, show that a similar profile to that of 1′ compression was followed i.e., strain hardening to a peak flow stress followed by flow softening. The peak flow stresses and extent of flow softening increased with strain rate as in the 1' compression for each material. As Fig. 8 indicates at a strain rate of 0.001 s^{-1} all the material conditions showed a near steady-state flow stress, with IHH giving the lowest result at 40–45 MPa.

From Fig. 8b and Table 5, IHH shows the highest *m* value at 0.32, THH showing the lowest from σ_{pfs} in 2″ compression at 0.29. IHH shows the largest degree of flow softening at a strain (ε) of 0.7 (equivalent of 50% compression), at 0.001 s^{-1}. For strain rates 0.01 and 0.1 s^{-1} the greatest extent of flow softening is seen in the HIP material - this being the case even with the highest flow stress at 0.01 s^{-1}. All material conditions show stable material flow under the 2" compression conditions.

4. Discussion

First, the distinction between the aims of primary and secondary processing should be made. Successful primary compression, seen as equivalent to ingot breakdown, or forming a pre-form in this study, looks to return a crack-free, isotropic behaving microstructure ready for secondary processing. To achieve this, pre-compression processing should aim to deliver a material that responds efficiently to deformation. An efficient response to primary compression includes returning a material with high lamellar globularisation, and so high X-DRX. Secondary processing covers high deformation processes such as hot rolling or isothermal closed-die forging, these techniques require a microstructure capable of strain rate sensitivity of ≥0.3 [4,27–31].

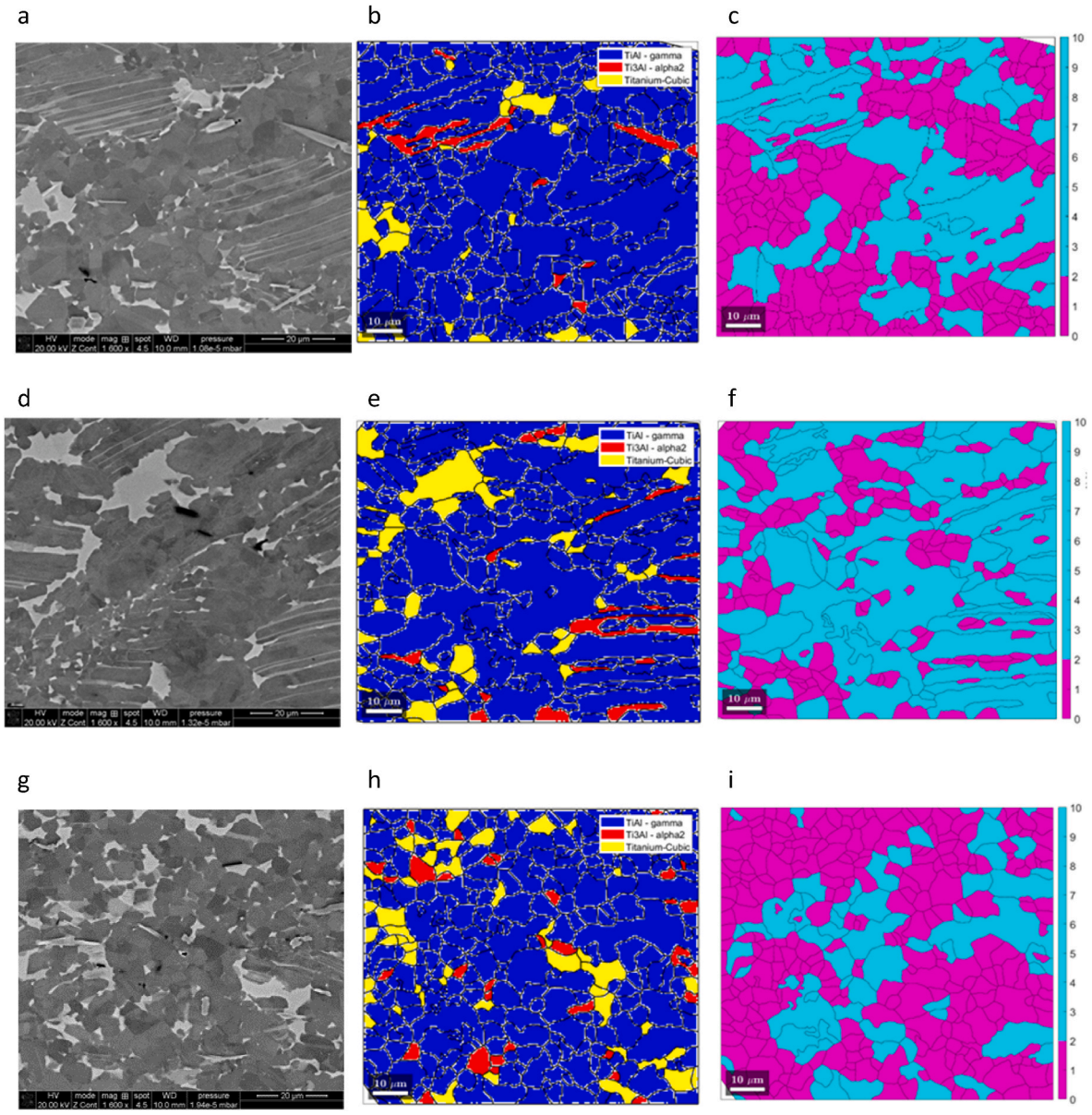

Fig. 5. SEM-BSE (left) with EBSD used to give maps of phase map (middle); blue is γ, red is α_2, yellow is β, X-DRX (Right); pink is the recrystallised fraction, light blue is deformed, after 50% compression at 1100 °C, 0.001 s^{-1}, of 45XD alloy in HIP (a, b, c), THH (d, e, f), IHH (g, h, i) condition at 1600x magnification.

Table 4
Phase, morphology, X-DRX and grain area fraction ≤50 μm^2 shown for each material after 50% primary compression at 1100 °C and 0.001, 0.005 and 0.01 s^{-1} calculated from a combination of OM, BSE and EBSD analysis.

45XD material condition (s^{-1})	α_2 lam (%)	β lam (%)	γ lam (%)	α_2 eq (%)	β eq (%)	γ eq (%)	Lamellar content (%)	X-DRX (%)	Grain area fraction ≤50μm^2 (%)
HIP 0.001	0.4	1.8	21.5	1.0	5.2	62.5	25.6	52.6	57.1
HIP 0.005	1.1	1.6	36.4	1.5	2.2	47.6	43.3	34.7	65.7
HIP 0.01	0.7	1.9	39.7	0.7	2.1	45.3	46.7	39.1	60.2
THH 0.001	2.4	3.3	38.3	2.9	4.0	45.7	45.6	29.6	42.0
THH 0.005	3.3	3.2	42.4	3.2	3.0	40.6	51.1	35.9	46.5
THH 0.01	1.7	5.6	33.4	1.6	5.4	32.6	50.6	32.7	48.0
IHH 0.001	0.5	1.6	14.6	1.9	7.0	62.4	18.9	67.1	68.3
IHH 0.005	0.7	3.5	30.7	1.1	5.4	48.3	38.9	37.8	55.5
IHH 0.01	1.9	2.3	46.0	1.5	1.8	36.0	56.1	31.7	62.3

4.1. Assessment of pre-compression microstructure

In this study hot isostatic pressing (HIP) was used to consolidate all material, reducing any casting porosity. The HIP temperature for this alloy is high in the α+γ region, within 20 °C of the α transus according to Fig. 1b. The influence of this process on the microstructure of titanium aluminides has been explored by a number of investigators for both finishing of cast parts and as preparation for further processing [32–34].

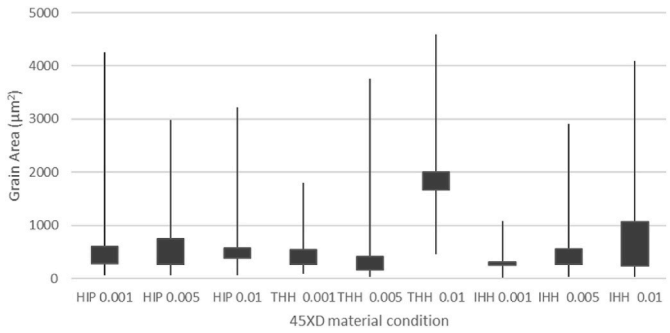

Fig. 6. Lamellar grain area analysis of maximum, minimum and interquartile range of each material condition after 50% primary compression at 1100 °C and 0.001, 0.005 and 0.01 s^{-1}.

Fig. 2a and microstructural details from Table 2 and Fig. 3, show a nearly fully lamellar microstructure after HIP.

The traditional HIP and homogenisation (THH) route includes a separate homogenisation heat treatment in the single α phase and is well established to return a fully lamellar and elementally homogeneous microstructure [10,11]. A decrease in the brittle β lamellar and equiaxed morphologies is seen from this heat treatment, with β stabilising elements being distributed homogeneously [25].

However, a growth in γ_{eq} morphologies is seen compared to IHH. This is likely to be due to the slow furnace cooling and time spent within γ dominant phase regions, Fig. 1b, from both HIP and HMG processes. This has led to lamellar grain growth, coarsening of γ laths and separate globular γ grain growth i.e. has reduced structural homogeneity, as seen in Fig. 2c and quantified in Table 2 and Fig. 3. This lamellar grain growth is not thought to be due to high temperature HMG, but due to the boride content of this alloy restricting grain growth [32,35].

The integrated HIP and homogenisation (IHH) route see both HIP and HMG times and temperatures being comparable with THH, the differences being that each stage is under pressure within the HIP vessel and the THH treatment has an intervening cooling stage. *Zhang, Dehm and Clemens'* investigations into the HIP and HMG of peritectic alloys found both pressure and α phase HMG essential to removing B2/β_0, but came with excessive grain growth [25]. As mentioned, the boride content of the alloy used in this study is higher, at 0.84 at%, than the alloy used in their study, 0.27 at%, and so restrains the grain growth associated with α phase heat treatment more effectively. The combination of temperature and pressure also generates a reduction in the overall β morphology content versus both HIP and THH routes. *Zhang, Dehm and Clemens* commented that pressure probably reduces the activation barrier to decompose B2/β_0.

In addition to this, the single cooling stage, as opposed to two cooling stages of THH, would explain the lack of γ morphology coarsening seen in IHH. The IHH process returned a more fully lamellar microstructure in comparison to HIP and THH routes, with a higher overall lamellar content and a tighter spread of lamellar grain area values, giving a more homogeneous lamellar microstructure in comparison, see Fig. 3.

4.2. Assessment of primary compression behaviour

Each stress-strain curve of Fig. 4a, follows a similar pattern; work hardening to a peak flow stress, due to a build-up of dislocation density, followed by flow softening. This behaviour is a characteristic of lamellar grain fragmentation in this material, this can be followed by DRX of this material with an increase in strain [36,37].

When considering the compression of lamellar material, DRX is often referred to as dynamic globularisation, as reviewed by Gao et al. for conventional Titanium alloys [38]. Similarities and differences between this and DRX for titanium aluminide alloys were identified by *Seetharaman and Semiatin* [31]. Recrystallisation, and to a lesser extent phase boundary bulging, were identified as the mechanisms of globularisation by *Zhang* et al. *in TiAl alloys*; this behaviour was further described by Tian et al. [17,39].

The X-DRX was calculated in this work through the GOS approach, seen in Fig. 7, calculated from EBSD data. GOS uses the average misorientation degree within grains, the misorientation spread in DRX grains is lower than that of deformed grains, an approach identified by Hadadzadeh et al. [18]. This has been applied to work on TiAl alloys to validate DRX predictive modelling and form processing maps, using ≤2° as the benchmark for DRX grains, as has been used here [40,41]. However, both of these latter studies assume the microstructure is homogeneous; with powder metallurgy this is more likely to be the case than for large cast ingot work.

Semiatin, Seetharaman and Weiss reviewed earlier work looking at the relationship between starting microstructure, flow softening rate, recrystallisation and flow localisation [42]. The authors identified that the lamellar characteristics, especially differences in lamellar grain area, were the most significant factor influencing the flow stress.

This is apparent with IHH material, presenting the lowest and tightest range of lamellar grain area values, generating lower peak flow stresses from the slower strain rates; 0.001 and 0.005 s^{-1}. However, at the faster strain rate of 0.01 s^{-1} the flow stress for IHH is the highest out of the three material conditions: smaller grain structures giving higher flow stresses. This is probably due to resistance to DRX/globularisation at these speeds, globularisation kinetics being enhanced by slower strain rates. This aligns with the observations of *Semiatin, Seetharaman and Ghosh* [43].

The relatively high flow stress from the HIP material at slow strain rates could be due to the same mechanism seen in creep and fatigue trials. Segregation leads to heavy alloying elements and interstitials being preferentially gettered into the α_2, or forming B2/β_0, from γ. This means the α_2 and β is less prone to globularisation when under strain, due to slower dissolution of α_2 into γ and solid solution hardening effects [44–46].

For each strain rate, IHH leads to the lowest flow stress after a strain of 0.7. Once this stress-strain profile levels out DRX/globularisation is sluggish due to lamellar grains orientating perpendicular to compression axis. The level of this flow stress is related to the extent of recrystallised material and its size [31].

Incorporating the contributing factors discussed above, Fig. 4b shows the 1' strain rate sensitivity (m) of IHH to be greatest, HIP to be lowest at σ_{pfs}, this trend does not change with strain [43].

4.3. Assessment of primary compression microstructure

Compression leaves all material in a refined condition in terms of lamellar grain area and content, as seen in the maps in Fig. 5, and in Table 4 and.

Fig. 6. However, all material conditions still retain large lamellar grains. Remnant lamellar grains show a mean grain area between 2000 and 4000 μm^2. The orientation of any remnant lamellar grains appeared to align perpendicular to compression, as found by other researchers [16,17,19].

The higher fraction of small equiaxed γ compared to the starting microstructures suggests that lamellar colonies near or parallel to the compression axis have been globularised. With an initial refined lamellar grain structure comes an increase in grain boundary density, these grain boundaries being the nucleation site for the formation of globular morphologies. This can be seen in the compression sample images; each remnant lamellar grain is necklaced by globular grains; see Fig. 5 a and d.

This is quantified by the X-DRX and lamellar content values in Table 4 and.

Fig. 6. The fraction and size of the recrystallised material is an important factor in further workability as identified by *Zhang* et al. [17]. The fraction of grains under 50 μm^2, identified by grain distribution

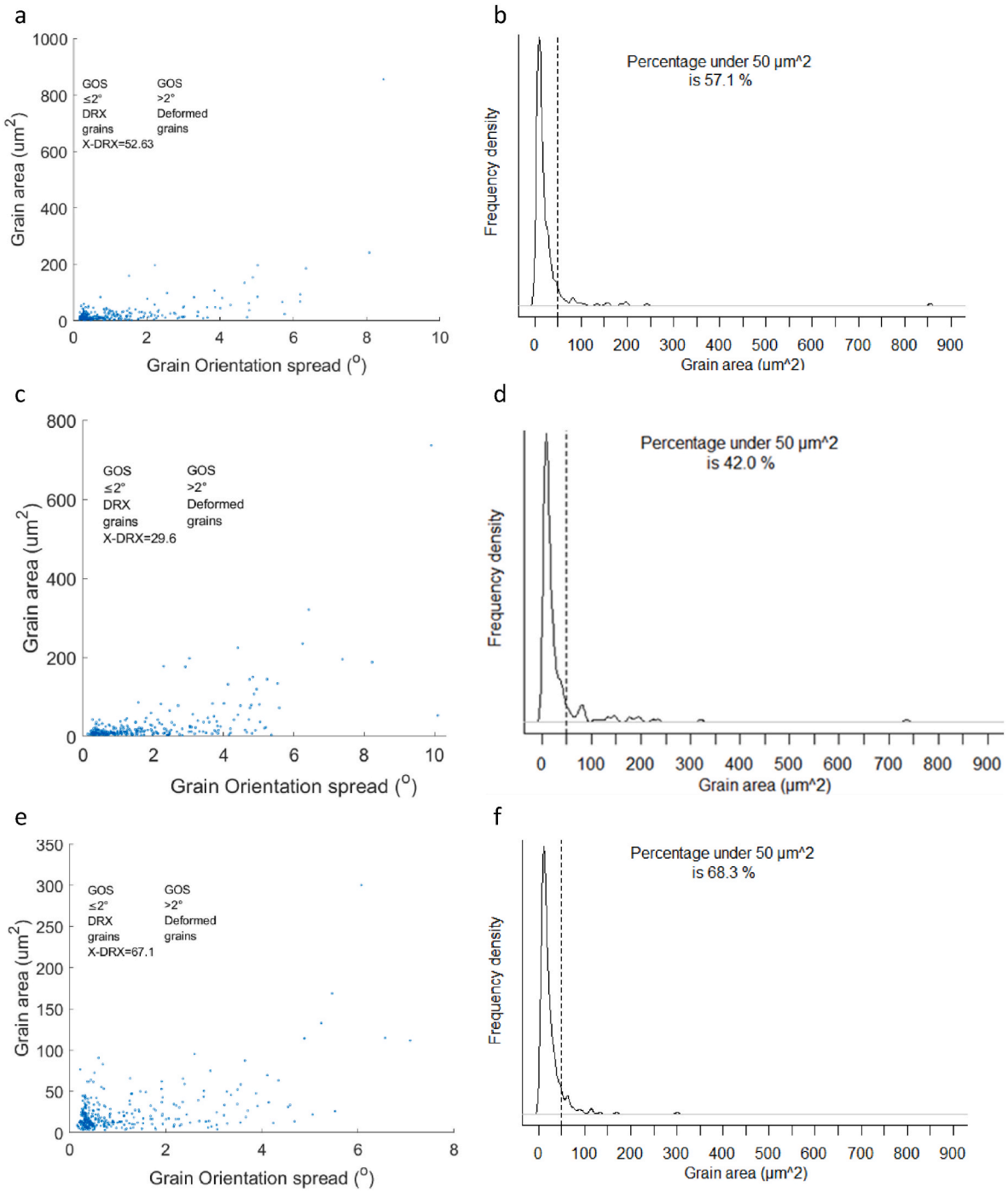

Fig. 7. Plots calculating the DRX fraction from the GOS approach on the left, grain area frequency density on the right, for each material condition after 50% primary compression at 1100 °C and 0.001 s^{-1}, (a, b) HIP, (c, d) THH, (e, f) IHH.

plots in Fig. 7b, d, f, look to quantify this and distinguish the relationship between this and *m* from secondary compression of this material.

Table 4 and Fig. 6 show that the lamellar grain area increases and X-DRX decreases with an increase in strain rate for IHH and THH material, though the case with the HIP material is not as clear. The efficiency of globularisation/recrystallisation is reduced with an increase in strain rate for THH and IHH, in common with Ti based lamellar materials, as discussed above [43].

In the case of HIP material, the lack of a clear trend in lamellar grain area with increasing strain rate could be due to a combination of factors. To start, the elemental segregation present from the lack of homogenisation means globularisation is sluggish as discussed in 4.2. There is also a high γ_{eq} and low lamellar content in the starting HIP microstructure. This favours micro-buckling/rotation rather than globularisation, explaining the higher lamellar grain area values and the higher lamellar fraction, and so in turn lower extent of X-DRX material seen from 50% compression of HIP when compared to IHH, in Table 4 [31,47]. Globularisation favours lamellar to lamellar grain boundaries, as seen in the IHH microstructure pre-compression, this was also noted by *Seetharaman and Semiatin* [31].

However, even with a HMG stage, the THH material returned a lower X-DRX value than either HIP or IHH at 0.001 s^{-1}, and similar values for lamellar fraction and X-DRX for 0.005 and 0.01 s^{-1}. This perhaps is a consequence of having the highest starting lamellar grain area; Fig. 3,

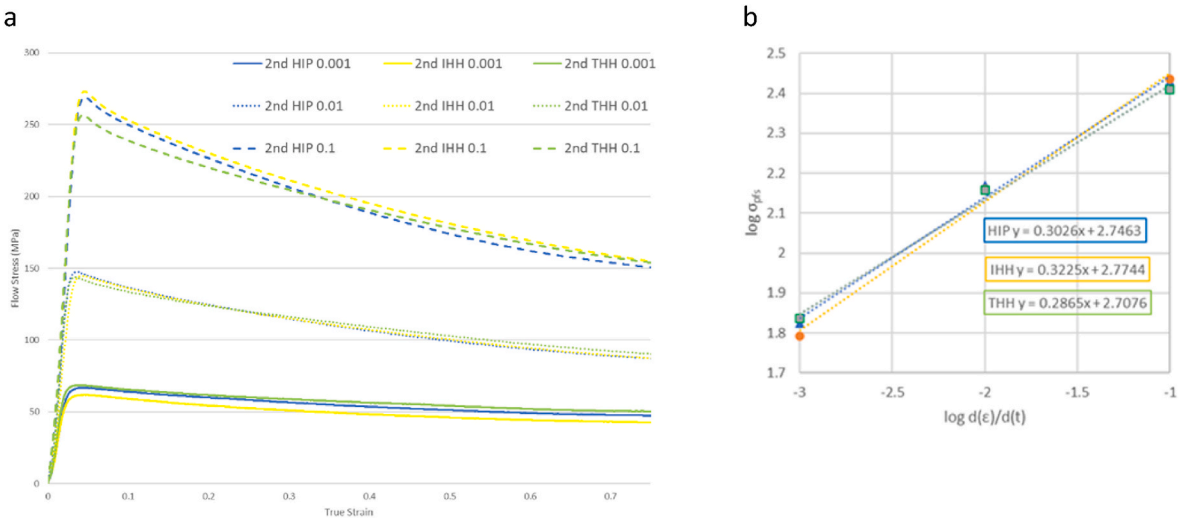

Fig. 8. Secondary stress-stain curves (a), secondary compression at 1100 °C to 50% at 0.001, 0.01 and 0.1 s^{-1} over 870, 87 and 8.7 s respectively. Calculation of strain rate sensitivity (m) for each material for secondary compression (b).

Table 5
Peak flow stress, strain rate sensitivity for each material condition over secondary compression.

Material	HIP			IHH			THH		
Strain rate (s^{-1})	0.001	0.01	0.1	0.001	0.01	0.1	0.001	0.01	0.1
2″ σ_{pfs}-(MPa)	66.8	147.6	269.0	61.9	144.7	273.1	68.6	144.0	256.6
2″ m (σ_{pfs})	0.30			0.32			0.29		

due to the slow cooling of both HIP and HMG stages. The relationship between maximum lamellar grain area values and X-DRX is shown in Fig. 9, and is in agreement with the work of others identifying the effect of large lamellar colonies on globularisation kinetics [43].

From a phase fraction point of view, the increase in β content post 1′ compression is of concern for further processing of IHH and THH material. As seen in 1' compression of HIP material, a high β content appears to contribute to high flow stress. This increase in β post compression, could be due to the compression temperature lying within a spike in β_0/B2 fraction, as shown in CALPHAD, Fig. 1b. This increase in β being more noticeable due to the homogenised microstructure of the initial THH and IHH microstructures, segregation promoting β formation in HIP material. An intermediate heat treatment could prove useful to alter this phase fraction to a more beneficial ratio, as identified by other researchers [4,10,17].

4.4. Assessment of secondary compression behaviour

The relationship between the primary upset microstructure and secondary compression behaviour is primarily dictated by X-DRX;

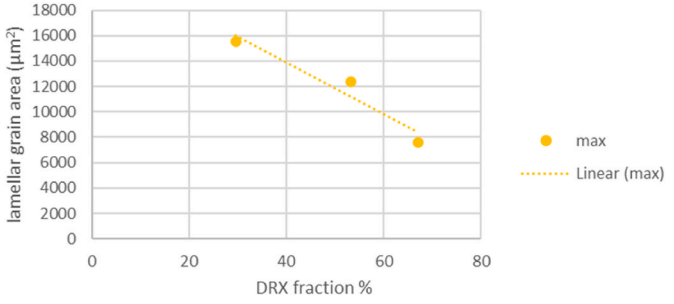

Fig. 9. Relationship between maximum pre-compression lamellar grain area and DRX fraction returned from primary compression at 0.001 s^{-1}.

Fig. 10a. Factors including the remnant lamellar grain area and fraction, as well as phase fraction, shown in Fig. 10b, c and d, appear to play a role, but to a lesser extent. IHH shows the highest value for *m,* THH the lowest, Fig. 8b. THH material does not achieve the minimum *m* of ≥0.3. Explanations for this can be seen in.

Fig. 6 and 7; THH has the largest remnant lamellar grains as well as lowest X-DRX and grain area fraction under ≤50 μm^2. The reasoning for this was discussed in section 4.3. This is not to say that the THH process cannot be adapted to produce relatively refined lamellar grains, i.e. by cooling rate control [48].

Secondary compression stress-strain curves, Fig. 8a, follow the same pattern as that seen in primary compression, described in 4.2. Notably, compression at 0.001 s^{-1} returns a poorly defined σ_{pfs} and steady state stress gained at a strain of 0.5, with little flow softening for all material conditions at 1100 °C. IHH material showed the lowest steady state stress at which a quasi-constant structure is assumed to have been reached [27]. This is not achieved with faster strain rates. This indicates that each material is still sensitive to processing conditions in terms of dynamic recrystallisation kinetics and extent. It is likely that higher temperatures would increase *m*, due to nucleation and growth of dynamic recrystallised grains being temperature driven, easing dislocation destruction [40].

4.5. Summary of the IHH process in respect to workability

This work examines the suitability of the IHH process to facilitate thermo-mechanical processing under the conditions described for this boride containing alloy. Reducing the time spent at temperatures high in the γ+α lamellar phase field, due to the single cooling stage of the IHH process, reduces the window for lamellar grain and lath coarsening, both of which are detrimental to globularisation in primary compression. Studies by Seo et al. on 45XD have shown the coarsening effect of slow furnace cooling rates on both grain size and lath thickness of fully lamellar microstructures [49]. However, fine lamellar morphologies also have to be avoided as these are also detrimental to globularisation

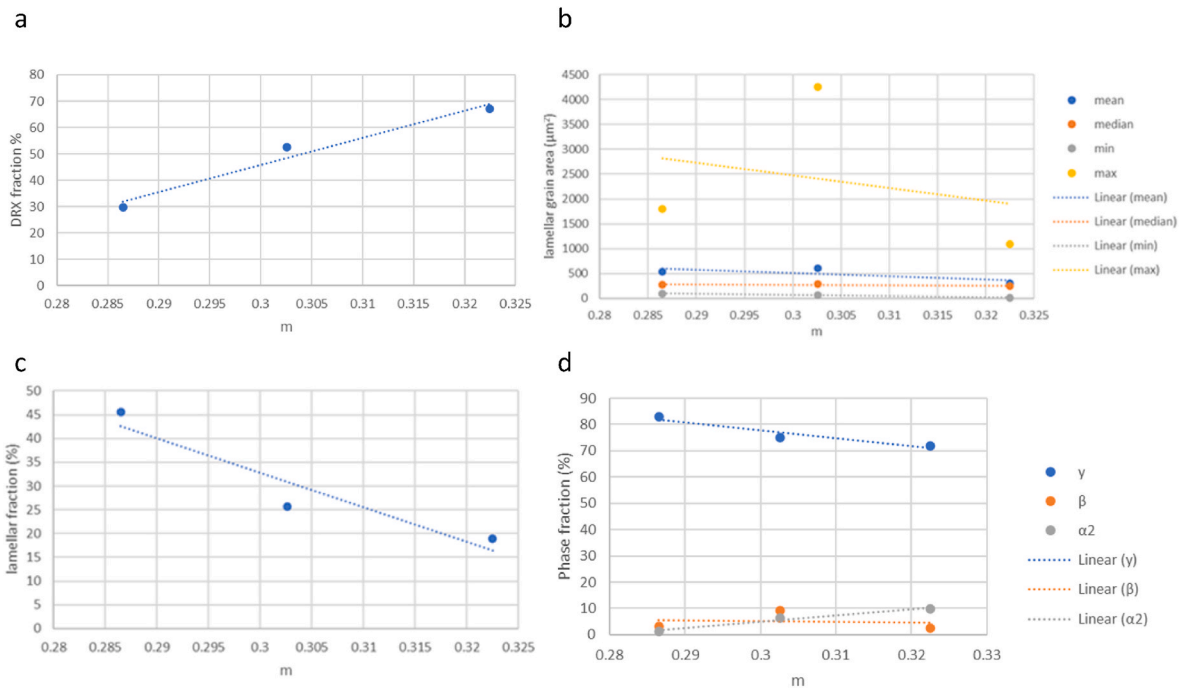

Fig. 10. Relationship between secondary strain rate sensitivity and, (a) primary compression DRX fraction, (b) primary compression lamellar grain area, (c) primary compression lamellar content, (d) primary compression phase, from secondary compression of HIP, IHH and THH at 1100 °C, 0.001 s^{-1}.

kinetics [16,17]. A compromise is clearly required.

With regard to the pressure used in IHH, *Chen* et al. concluded that the isostatic pressure had no bearing on morphology evolution, but suppressed microcrack formation [26]. *Zhang, Dehm and Clemens,* suggested that pressure reduced the activation barrier required for decomposition of the B2/β_0 in subsequent HMG [25]. *Zhang, Dehm and Clemens* using a similar triple phase containing alloy to that used in the present study. The work presented here shows no identifiable effect of pressure on the morphology present but there is evidence for the decomposition of the B2/β_0 phase, as displayed in Table 2. Based on the results from the research reported here, it can also be proposed that cooling between HIP and HMG is unnecessary and can be detrimental in terms of further workability. IHH could thus be an alternative approach for pre-compression processing for boride containing, fully lamellar, peritectic TiAl alloys like 45XD.

5. Conclusions

The aim of this study was to understand how consolidation and homogenisation, as well as the possibility of integrating the two processes, influences the pre-compression 45XD microstructure and its subsequent compression behaviour and microstructure. The following conclusions for this alloy were drawn.

- Conventional hot isostatic pressing to remove porosity is clearly essential but does not generate a microstructure optimised to remove the lamellar content during subsequent primary compression.
- The ideal pre-compression microstructure for efficient globularisation is refined, fully lamellar, with elemental homogeneity, with a reduced B2/β_0 content. This makes a heat treatment above the α transus necessary.
- High temperature heat treatments (above the α transus) can cause lamellar grain growth, the presence of which has been identified in these studies as a major cause of slowing globularisation and so reducing dynamic recrystallised grain fraction. This reduces strain rate sensitivity in secondary processing.
- Pressure and temperature during the integrated HIP and homogenisation (IHH) process reduced B2/β_0 content compared to that seen in the traditional HIP and homogenisation (THH) process and HIP alone. Integrating the two processes also removes slow cooling from homogenisation, returning a more fully lamellar microstructure, so improving the conditions for globularisation. This resulted in a higher dynamic recrystallised fraction from primary processing, so higher strain rate sensitivity and better workability in secondary processing.

CRediT author statement

Sean Peters: Conceptualization, Methodology, Investigation, Data Curation, Writing- Original draft preparation. Marcos Perez: Conceptualization and Supervision. Paul Blackwell: Supervision, Funding acquisition and Writing- Reviewing and Editing.

Declaration of competing interest

The authors declare that they have no known competing financial interests or personal relationships that could have appeared to influence the work reported in this paper.

Data availability

Data will be made available on request.

Acknowledgements

The authors would like to acknowledge the support provided by TIMET for constructive discussion and donating the material, and the funding supported by the Core membership at the Advanced Forming Research Centre (AFRC) and Scottish Research Partnership in Engineering (SRPe).

References

[1] D.M. Dimiduk, Gamma titanium aluminide alloys - an assessment within the competition of aerospace structural materials, Mater. Sci. Eng. 263 (1999) 281–288, https://doi.org/10.1016/s0921-5093(98)01158-7.

[2] F.J. Appel, J.D. Paul, M. Oehring, Gamma Titanium Aluminides, 1981.

[3] F. Appel, M. Oehring, J.D.H. Paul, C. Klinkenberg, T. Carneiro, Physical aspects of hot-working gamma-based titanium aluminides, Intermetallics 12 (2004) 791–802, https://doi.org/10.1016/j.intermet.2004.02.042.

[4] G.E. Fuchs, The effect of processing on the hot workability of Ti-48Al-2Nb-2Cr alloys, Metall. Mater. Trans. A Phys. Metall. Mater. Sci. 28 (1997) 2543–2553, https://doi.org/10.1007/s11661-997-0012-y.

[5] M. Yamaguchi, H. Inui, S. Yokoshima, K. Kishida, D.R. Johnson, Recent progress in our understanding of deformation and fracture of two-phase and single-phase TiAl alloys, Transit. 213 (1996) 25–31.

[6] Y.Y. Chen, B.H. Li, F.T. Kong, Microstructural refinement and mechanical properties of Y-bearing TiAl alloys, J. Alloys Compd. 457 (2008) 265–269, https://doi.org/10.1016/j.jallcom.2007.03.050.

[7] F. Kong, Y. Chen, F. Yang, Effect of heat treatment on microstructures and tensile properties of as-forged Ti-45Al-5Nb-0.3Y alloy, Intermetallics 19 (2011) 212–216, https://doi.org/10.1016/j.intermet.2010.08.012.

[8] F. Kong, N. Cui, Y. Chen, X. Wang, N. Xiong, Characterization of hot deformation behavior of as-forged TiAl alloy, Intermetallics 55 (2014) 66–72, https://doi.org/10.1016/j.intermet.2014.07.010.

[9] H.Z. Niu, Y.Y. Chen, F.T. Kong, J.P. Lin, Microstructure evolution, hot deformation behavior and mechanical properties of Ti-43Al-6Nb-1B alloy, Intermetallics 31 (2012) 249–256, https://doi.org/10.1016/j.intermet.2012.07.016.

[10] S.L. Semiatin, V. Seetharaman, V.K. Jain, Microstructure development during conventional and isothermal hot forging of a near-gamma titanium aluminide, Metall. Mater. Trans. 25 (1994) 2753–2768, https://doi.org/10.1007/BF02649227.

[11] S.L. Semiatin, V. Seetharaman, D.M. Dimiduk, K.H.G. Ashbee, Phase transformation behavior of gamma titanium aluminide alloys during supertransus heat treatment, Metall. Mater. Trans. A Phys. Metall. Mater. Sci. 29 (1998) 7–18, https://doi.org/10.1007/s11661-998-0154-6.

[12] G.E. Fuchs, Supertransus processing of TiAl-based alloys, Metall. Mater. Trans. A Phys. Metall. Mater. Sci. 29 (1998) 27–36, https://doi.org/10.1007/s11661-998-0156-4.

[13] A. Kościelna, W. Szkliniarz, Effect of cyclic heat treatment parameters on the grain refinement of Ti–48Al–2Cr–2Nb alloy, Mater. Char. 60 (2009) 1158–1162, https://doi.org/10.1016/j.matchar.2009.03.008.

[14] J.K. Kim, J.H. Kim, J.Y. Kim, S.H. Park, S.W. Kim, M.H. Oh, S.E. Kim, Producing fine fully lamellar microstructure for cast γ-TiAl without hot working, Intermetallics 120 (2020), 106728, https://doi.org/10.1016/j.intermet.2020.106728.

[15] E. Schwaighofer, H. Clemens, S. Mayer, J. Lindemann, J. Klose, W. Smarsly, V. Güther, Microstructural design and mechanical properties of a cast and heat-treated intermetallic multi-phase γ-TiAl based alloy, Intermetallics 44 (2014) 128–140, https://doi.org/10.1016/j.intermet.2013.09.010.

[16] R.M. Imayev, V.M. Imayev, M. Oehring, F. Appel, Microstructural evolution during hot working of Ti aluminide alloys: influence of phase constitution and initial casting texture, Metall. Mater. Trans. 36 (2005) 859–867, https://doi.org/10.1007/s11661-005-0199-8.

[17] W.J. Zhang, U. Lorenz, F. Appel, Recovery, recrystallization and phase transformations during thermomechanical processing and treatment of TiAl-based alloys, Acta Mater. 48 (2000) 2803–2813, https://doi.org/10.1016/S1359-6454(00)00093-8.

[18] A. Hadadzadeh, F. Mokdad, M.A. Wells, D.L. Chen, A new grain orientation spread approach to analyze the dynamic recrystallization behavior of a cast-homogenized Mg-Zn-Zr alloy using electron backscattered diffraction, Mater. Sci. Eng. 709 (2018) 285–289, https://doi.org/10.1016/j.msea.2017.10.062.

[19] A.J. Palomares-García, M.T. Pérez-Prado, J.M. Molina-Aldareguia, Effect of lamellar orientation on the strength and operating deformation mechanisms of fully lamellar TiAl alloys determined by micropillar compression, Acta Mater. 123 (2017) 102–114, https://doi.org/10.1016/j.actamat.2016.10.034.

[20] T. Tetsui, A newly developed hot worked TiAl alloy for blades and structural components, Scripta Mater. 47 (2002) 399–403, https://doi.org/10.1016/S1359-6462(02)00158-6.

[21] Q. Wang, R. Chen, Y. Yang, S. Wu, J. Guo, H. Ding, Y. Su, H. Fu, Effects of lamellar spacing on microstructural stability and creep properties in β-solidifying γ-TiAl alloy by directional solidification, Mater. Sci. Eng. 711 (2018) 508–514, https://doi.org/10.1016/j.msea.2017.11.080.

[22] T. Li, G. Liu, M. Xu, B. Wang, T. Fu, Z. Wang, R.D.K. Misra, Flow stress prediction and hot deformation mechanisms in Ti-44Al-5Nb-(Mo, V, B) alloy, Mater. 11 (2018), https://doi.org/10.3390/ma11102044.

[23] F. Appel, H. Clemens, F.D. Fischer, Modeling concepts for intermetallic titanium aluminides, Prog. Mater. Sci. 81 (2016) 55–124, https://doi.org/10.1016/j.pmatsci.2016.01.001.

[24] G. Molénat, B. Galy, M. Musi, L. Toualbi, M. Thomas, H. Clemens, J.P. Monchoux, A. Couret, Plasticity and brittleness of the ordered βo phase in a TNM-TiAl alloy, Intermetallics 151 (2022), https://doi.org/10.1016/j.intermet.2022.107653.

[25] D. Zhang, G. Dehm, H. Clemens, Effect of heat-treatments and hot-isostatic pressing on phase transformation and microstructure in a β/B2 containing γ-TiAl based alloy, Scripta Mater. 42 (2000) 1065–1070, https://doi.org/10.1016/S1359-6462(00)00341-9.

[26] L. Chen, L. Zhu, Y. Guan, B. Zhang, J. Li, Tougher TiAl alloy via integration of hot isostatic pressing and heat treatment, Mater. Sci. Eng. 688 (2017) 371–377, https://doi.org/10.1016/j.msea.2017.02.028.

[27] A.K. Ghosh, On the measurement of strain-rate sensitivity for deformation mechanism in conventional and ultra-fine grain alloys, Mater. Sci. Eng. 463 (2007) 36–40, https://doi.org/10.1016/j.msea.2006.08.122.

[28] N. Bibhanshu, A. Bhattacharjee, S. Suwas, Hot deformation response of titanium aluminides Ti–45Al-(5, 10)Nb-0.2B-0.2C with pre-conditioned microstructures, J. Alloys Compd. 832 (2020), 154584, https://doi.org/10.1016/j.jallcom.2020.154584.

[29] S.L. Semiatin, A. Force, M. Directorate, ASM Handbook: Metalworking: Bulk Forming, 2005, https://doi.org/10.1361/asmhba0003971.

[30] R.K. Gupta, S.V.S. Narayana Murty, B. Pant, V. Agarwala, P.P. Sinha, Hot workability of γ+α 2 titanium aluminide: development of processing map and constitutive equations, Mater. Sci. Eng. 551 (2012) 169–186, https://doi.org/10.1016/j.msea.2012.05.005.

[31] V. Seetharaman, S.L. Semiatin, Effect of the lamellar grain size on plastic flow behavior and microstructure evolution during hot working of a gamma titanium aluminide alloy, Metall. Mater. Trans. A Phys. Metall. Mater. Sci. 33 (2002) 3817–3830, https://doi.org/10.1007/s11661-002-0254-7.

[32] C. Yang, D. Hu, X. Wu, A. Huang, M. Dixon, Microstructures and tensile properties of hot isostatic pressed Ti4522XD powders, Mater. Sci. Eng. 534 (2012) 268–276, https://doi.org/10.1016/j.msea.2011.11.068.

[33] G. Wegmann, R. Gerling, F.P. Schimansky, H. Clemens, A. Bartels, High-temperature mechanical properties of hot isostatically pressed and forged gamma titanium aluminide alloy powder, Intermetallics 10 (2002) 511–517, https://doi.org/10.1016/S0966-9795(02)00026-2.

[34] R.J. Simpkins, M.P. Rourke, T.R. Bieler, P.A. McQuay, The effects of HIP pore closure and age hardening on primary creep and tensile property variations in a TiAl XD^{TM} alloy with 0.1 wt.% carbon, Mater. Sci. Eng. 463 (2007) 208–215, https://doi.org/10.1016/j.msea.2006.09.114.

[35] D. Hu, Role of boron in TiAl alloy development: a review, Rare Met. 35 (2016) 1–14, https://doi.org/10.1007/s12598-015-0615-1.

[36] S.L. Semiatin, A. Force, M. Directorate, ASM Handbook: Metalwork.: Bulk Forming 14A (2005) 888.

[37] J.C.F. Millett, J.W. Brooks, I.P. Jones, Assessment and modelling of isothermal forging of intermetallic compounds Part 1 - TiAl, Mater. Sci. Technol. 15 (1999) 697–704, https://doi.org/10.1179/026708399101506292.

[38] P. Gao, M. Fu, M. Zhan, Z. Lei, Y. Li, Deformation behavior and microstructure evolution of titanium alloys with lamellar microstructure in hot working process: a review, J. Mater. Sci. Technol. 39 (2020) 56–73, https://doi.org/10.1016/j.jmst.2019.07.052.

[39] S. Tian, H. Jiang, W. Guo, G. Zhang, S. Zeng, Hot deformation and dynamic recrystallization behavior of TiAl-based alloy, Intermetallics 112 (2019), 106521, https://doi.org/10.1016/j.intermet.2019.106521.

[40] Z. Wan, Y. Sun, L. Hu, H. Yu, Dynamic softening behavior and microstructural characterization of TiAl-based alloy during hot deformation, Mater. Char. 130 (2017) 25–32, https://doi.org/10.1016/j.matchar.2017.05.022.

[41] X. Chen, B. Tang, D. Liu, B. Wei, L. Zhu, R. Liu, H. Kou, J. Li, Dynamic recrystallization and hot processing map of Ti-48Al-2Cr-2Nb alloy during the hot deformation, Mater. Char. 179 (2021), 111332, https://doi.org/10.1016/j.matchar.2021.111332.

[42] I.W.S.L. Semiatin, V. Seetharaman, Hot workability of titanium and titanium aluminide alloys—an overview, Mater. Sci. Eng. 243 (1998) 1–24.

[43] S.L. Semiatin, V. Seetharaman, A.K. Ghosh, Plastic flow, microstructure evolution, and defect formation during primary hot working of titanium and titanium aluminide alloys with lamellar colony microstructures, Philos. Trans. R. Soc. A Math. Phys. Eng. Sci. 357 (1999) 1487–1512, https://doi.org/10.1098/rsta.1999.0386.

[44] M. Kastenhuber, B. Rashkova, H. Clemens, S. Mayer, Enhancement of creep properties and microstructural stability of intermetallic β-solidifying γ-TiAl based alloys, Intermetallics 63 (2015) 19–26, https://doi.org/10.1016/j.intermet.2015.03.017.

[45] J. Lapin, T. Pelachová, M. Dománková, Long-term creep behaviour of cast TiAl-Ta alloy, Intermetallics 95 (2018) 24–32, https://doi.org/10.1016/j.intermet.2018.01.013.

[46] J. Bresler, S. Neumeier, M. Ziener, F. Pyczak, M. Göken, The influence of niobium, tantalum and zirconium on the microstructure and creep strength of fully lamellar γ/α 2 titanium aluminides, Mater. Sci. Eng. 744 (2019) 46–53, https://doi.org/10.1016/j.msea.2018.11.152.

[47] J.P. Monchoux, J. Luo, T. Voisin, A. Couret, Deformation modes and size effect in near-γ TiAl alloys, Mater. Sci. Eng. 679 (2017) 123–132, https://doi.org/10.1016/j.msea.2016.09.092.

[48] H. Zhu, D.Y. Seo, K. Maruyama, P. Au, Microstructural stability of fine-grained fully lamellar XD TiAl alloys by step aging, Metall. Mater. Trans. A Phys. Metall. Mater. Sci. 36 (2005) 1339–1351, https://doi.org/10.1007/s11661-005-0225-x.

[49] D. Seo, L. Zhao, J. Beddoes, Microstructural evolution during heat treatments in Ti-45 and 47Al–2Nb–2Mn+0.8vol.%TiB2 XDTM alloys, Mater. Sci. Eng. 329–331 (2002) 130–140, https://doi.org/10.1016/S0921-5093(01)01546-5.